

# In Situ Formation of Suspended Graphene Windows for Lab-Based XPS in Liquid and Gas Environments

Elizabeth S. Jones,<sup>[a]</sup> Charalampos Drivas,<sup>[b, c, d]</sup> Joshua S. Gibson,<sup>[a]</sup> Jack E. N. Swallow,<sup>[a, e]</sup> Leanne A. H. Jones,<sup>[a]</sup> Thomas D. J. Bricknell,<sup>[a]</sup> Matthijs A. van Spronsen,<sup>[e]</sup> Georg Held,<sup>[e]</sup> Mark A. Isaacs,<sup>[b, f]</sup> Christopher M. A. Parlett,<sup>[c, d]</sup> and Robert S. Weatherup<sup>\*[a, d, e]</sup>

Environmental cells sealed with photoelectron-transparent graphene windows are promising for extending X-ray photoelectron spectroscopy (XPS) to liquid and high-pressure gas environments for *in situ* and *operando* studies. However, the reliable production of graphene windows that are sufficiently leak-tight for extended measurements remains a challenge. Here we demonstrate a PDMS/Au(100 nm)-supported transfer method that reliably produces suspended graphene on perforated silicon nitride membranes without significant contamination. A yield of ~95% is achieved based on single-layer

graphene covering >98% of the holes in the silicon nitride membrane. Even higher coverages are achieved for stacked bilayer graphene, allowing wet etching (aqueous KI/I<sub>2</sub>) of the Au support to be observed in a conventional lab-based XPS system, thereby demonstrating the *in situ* formation of leak-tight, suspended graphene windows. Furthermore, these windows allow gas-phase measurements at close to atmospheric pressure, showing future promise for XPS under higher-pressure gas environments in conventional lab-based systems.

## Introduction

Observing the chemical state of catalyst surfaces whilst still in their reaction environment (*in situ*), or during the reaction itself (*operando*) is critical to understanding and rationally improving the performance of catalysts used in key sustainable technologies related to energy storage, conversion, and the decarbon-

isation of industrial processes.<sup>[1–7]</sup> In particular, pressure and temperature can greatly influence the state of a surface and the position of equilibrium of a reaction,<sup>[8,9]</sup> as described by Le Chatelier's principle. It is thus often not sufficient to perform "post-mortem" characterisation where the reaction is stopped and the sample inertly transferred to the measurement system, as the chemical state of the surface may be significantly altered.<sup>[3,10,11]</sup> Therefore, a pressing need exists to develop *in situ*

[a] E. S. Jones, Dr. J. S. Gibson, Dr. J. E. N. Swallow, Dr. L. A. H. Jones, T. D. J. Bricknell, Prof. R. S. Weatherup  
Department of Materials  
University of Oxford  
Parks Road  
Oxford  
OX1 3PH  
United Kingdom  
E-mail: robert.weatherup@materials.ox.ac.uk

[b] Dr. C. Drivas, Dr. M. A. Isaacs  
HarwellXPS  
Research Complex at Harwell  
Rutherford Appleton Labs  
Didcot  
Oxfordshire  
OX11 0FA  
United Kingdom

[c] Dr. C. Drivas, Dr. C. M. A. Parlett  
Department of Chemical Engineering  
University of Manchester  
Manchester  
M13 9PL  
United Kingdom

[d] Dr. C. Drivas, Dr. C. M. A. Parlett, Prof. R. S. Weatherup  
Catalysis Hub  
Research Complex at Harwell  
Rutherford Appleton Labs  
Didcot  
Oxfordshire  
OX11 0FA  
United Kingdom

[e] Dr. J. E. N. Swallow, Dr. M. A. van Spronsen, Prof. G. Held,  
Prof. R. S. Weatherup  
Diamond Light Source  
Didcot  
Oxfordshire  
OX11 0DE  
United Kingdom

[f] Dr. M. A. Isaacs  
Department of Chemistry  
University College London  
20 Gordon Street  
London  
WC1H 0AJ  
United Kingdom

Supporting information for this article is available on the WWW under <https://doi.org/10.1002/cctc.202400239>

© 2024 The Authors. ChemCatChem published by Wiley-VCH GmbH. This is an open access article under the terms of the Creative Commons Attribution License, which permits use, distribution and reproduction in any medium, provided the original work is properly cited.

and *operando* approaches for studying catalyst surfaces that are widely accessible to the catalysis research community.

X-ray photoelectron spectroscopy (XPS) is amongst the most widely-available, interface-sensitive methods for observing the chemical state of surfaces.<sup>[12]</sup> The limited inelastic mean free path (IMFP) of photoelectrons, on the one hand, gives rise to a high-degree of surface sensitivity ( $< 10$  nm).<sup>[13–15]</sup> However, it also means that vacuum conditions are typically required to avoid scattering of the emitted photoelectrons, making *in situ* or *operando* studies challenging to implement.<sup>[16]</sup> Nevertheless, Siegbahn *et al.* introduced approaches for studying low pressure gases and liquid jets by using differential pumping to extend the effective photoelectron IMFP as well as maintaining the photoelectron analyser at sufficiently low pressures.<sup>[17–19]</sup> The incorporation of multiple pumping stages, with electrostatic lenses to improve collection efficiency, allowed further increases in the accessible pressures.<sup>[20]</sup> These near ambient pressure (NAP)-XPS systems have been commercially available for over a decade and can routinely perform measurements at tens of mbar. However, this still falls far below the pressures of most industrial processes ( $> 1$  bar). Recently, by using tender/hard ( $> 2$  keV) X-ray sources to increase photoelectron kinetic energy, and thus IMFP, it has been possible to extend NAP-XPS to measure solid-liquid interfaces,<sup>[21,22]</sup> and surfaces in 1 bar gas environments.<sup>[23]</sup> However, photoionization cross-sections decrease with photon energy, making it challenging to measure light elements such as oxygen and carbon with sufficient signal-to-noise ratios on reasonable timescales.<sup>[5,21,24–26]</sup>

Enclosed environmental cells offer a promising alternative approach to enable *in situ* and *operando* XPS, avoiding the complexity and cost of NAP systems, and providing access to higher pressure ranges ( $> 1$  bar) whilst still using soft X-ray excitation.<sup>[5,6,27–37]</sup> The reaction environment is sealed behind a photoelectron transparent window (Figure 1A(i)), and can be varied with few constraints, while the analysis chamber containing the cell is maintained under vacuum conditions. Although XPS measurements have been performed using very thin silicon nitride ( $\text{SiN}_x$ ) or Si windows ( $\sim 15$  nm) to measure liquids in lab-based and synchrotron-based systems, they typically require the use of hard X-rays to provide photoelectrons with sufficient kinetic energy, and thus IMFP, to escape.<sup>[22,38,39]</sup> A number of studies have thus made use of suspended graphene windows, which have thicknesses below the IMFP of the photoelectrons produced by soft X-ray sources, and can be highly impermeable to gases.<sup>[40,41]</sup> The electron transparency of graphene windows also expands the possible detection methods for near edge X-ray absorption fine structure (NEXAFS) spectroscopy. Interface-sensitive electron yield can be measured by collecting electrons escaping through the graphene, rather than requiring a separate counter electrode within the reaction cell,<sup>[9]</sup> or being limited to the more bulk sensitive fluorescence yield.<sup>[16]</sup> However, defects and tears in the graphene can lead to leakage, and therefore studies to date have either used extremely small cell volumes,<sup>[30–32]</sup> or NAP systems.<sup>[33–35]</sup> The wider adoption of this approach requires leak-tight graphene windows to allow measurements under high pressure gas or even liquid within conventional lab-based XPS

systems with Al-K $\alpha$  sources. Conventional lab-based XPS systems are far more accessible than synchrotron facilities and usually lower cost than equivalent NAP-XPS systems. Therefore, by improving the manufacture of graphene windows there is an avenue to greatly increase the accessibility of *in situ* and *operando* XPS.

Chemical vapour deposition (CVD) can produce high-quality, single-layer graphene (SLG) over large areas on transition metal supports, such as Cu.<sup>[42–44]</sup> For use as a window, the SLG must be transferred to a suitable support, such as a perforated  $\text{SiN}_x$  membrane, without introducing significant tears, wrinkles, or contamination. Tears and wrinkles could result in leaks and potential weak areas susceptible to bursting under pressure, whilst contamination may affect the reaction being observed and complicate XPS/NEXAFS analysis. The most common method for transferring CVD graphene uses a polymer support layer, to minimise tearing.<sup>[41,45]</sup> However, swelling of the polymer in etchant solution, as well as thermal expansion/contraction during heating steps can result in significant wrinkling.<sup>[46]</sup> Furthermore, incomplete removal of the polymer can leave undesired contamination.<sup>[47,48]</sup> To avoid this, polymer-free transfer using a frame has been demonstrated, but this is typically more challenging and likely to introduce damage.<sup>[34,49]</sup> Instead, it would be ideal if a support layer could be used that is subsequently needed for the measurement being performed, as this would avoid introducing further contamination.

Here, we demonstrate a method to reliably produce suspended SLG and bilayer graphene (BLG) windows on perforated  $\text{SiN}_x$  membranes, by the transfer of CVD graphene using a 100 nm thick Au support layer, with an additional polydimethylsiloxane (PDMS) frame to minimise wrinkling.<sup>[50]</sup> BLG windows are sufficiently leak-tight to allow etching of the Au by an aqueous  $\text{KI/I}_2$  solution to be monitored in a conventional lab-based instrument. In contrast to previous studies, we thereby demonstrate XPS of high-vapour pressure liquids under constant flow without the need for hard X-rays or a differentially pumped analyser.<sup>[22,27,28,33–35,38]</sup> SLG windows are also shown to be effective in containing 1 bar gas environments within a NAP-XPS system over extended periods, enabling the study of changes in Cu nanoparticle (NP) oxidation state with gas. Characterisation with XPS, Raman and scanning electron microscopy (SEM) confirms the Au-supported transfer gives continuous SLG with low-levels of contamination. The reliability of this approach for producing windows with  $> 98\%$  of the holes in the  $\text{SiN}_x$  covered with SLG is  $\sim 95\%$ , with the hole coverage further improved by stacking SLG to produce BLG windows. We thus show that reliable production of leak-free SLG/BLG windows makes *in situ* measurements of liquid and high-pressure gas environments feasible in conventional lab-based XPS systems, offering much greater access to *in situ* and *operando* XPS capabilities.

## Results and Discussion

Conventional lab-based XPS measurements using a monochromated Al K $\alpha$  X-ray source (1486.7 eV) were performed using a

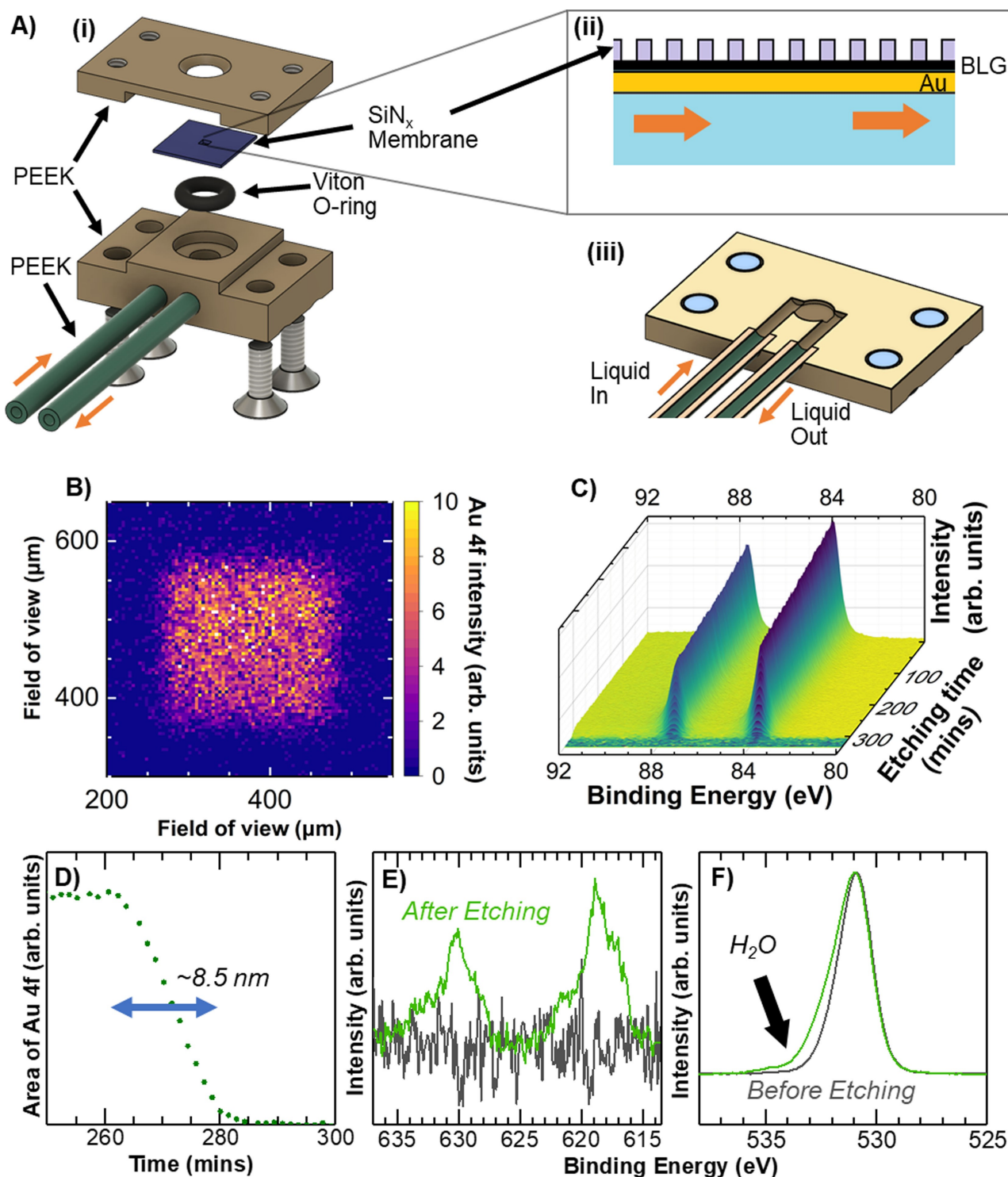


**Figure 1.** (A) Schematic of liquid flow cell made from PEEK used for conventional lab-based XPS. (i) Expanded view of the cell showing how the cell is sealed by the  $\text{SiN}_x$  membrane atop a Viton O-ring, (ii) shows BLG and Au suspended over the holes of the perforated  $\text{SiN}_x$  membrane, (iii) horizontal cross-section showing how liquid enters the cell through the PEEK tubes. (B) XPS map of the Au 4f signal at 84.0 eV (following charge calibration) for the perforated  $\text{SiN}_x$  window covered in BLG/Au. (C) Au 4f region varying over time whilst Au is etched with a  $\text{KI/I}_2$  solution. Peak positions have been energy calibrated with the Au 4f<sub>7/2</sub> peak at 84.0 eV. (D) Plot of the area of Au 4f peaks varying over time showing the etching of the final ~8.5 nm of Au. XPS regions comparing before (grey) and after (green) etching the Au with water and  $\text{KI/I}_2$  flowed through the cell, respectively, for the (E) I 3d region and (F) O 1s region.

custom liquid flow cell (Figure 1A(ii)) made from polyether ether ketone (PEEK) that is sealed by a  $\text{SiN}_x$  membrane pressed against a Viton O-ring. Inlet and outlet tubes made from PEEK

enable a flow of liquid such that reagents can be replenished (see Experimental Section in the Supplementary Information (SI) for detailed setup description). The membrane (500 $\times$ 500  $\mu\text{m}$ ,

200 nm thick SiN<sub>x</sub> on Si, Silson Ltd.) has a window area of 200×200 μm covered by an array of Ø1 μm holes arranged in a hexagonal grid at a pitch of 2 μm, resulting in porosity, and thus active area, of ~23%. These holes are sealed by the transfer of a Au(100 nm)/BLG film as described further below, with the membrane mounted such that the Au is directly exposed to the liquid environment (see Figure 1A(ii)). Alignment to the suspended Au(100 nm)/BLG region was achieved by spatially mapping the signal intensity from the Au 4f region (at a fixed binding energy of 84.0 eV after energy calibration) as shown in Figure 1B. The presence of Au from the transfer process assists with rapid alignment to the window region which can otherwise be time-consuming. Following this, distilled water was flowed (1.4 ml/min) into the cell for preliminary testing, with the XPS analysis chamber pressure remaining at ~3×10<sup>-7</sup> mbar. This chamber pressure is higher than usual for a conventional lab-based XPS system (<10<sup>-9</sup> mbar) due to the degassing of various components of the flow cell which were not baked prior to introduction into the XPS chamber. The water in the cell is then replaced with an Au etching solution: KI/I<sub>2</sub> (0.1 g of KI, 0.025 g of I<sub>2</sub> in 1 L of distilled water).<sup>[51,52]</sup> Figure 1C shows the change in the Au 4f signal over time whilst the etching solution was passed through the cell, with the binding energy corrected by setting the Au 4f<sub>7/2</sub> peak to 84.0 eV. The correction required is found to vary over time, which is likely a result of variations in charging as the cell is not in electrical contact with the spectrometer. The full width at half maximum (FWHM) of the Au 4f peaks did not vary throughout the experiments suggesting no intermediate species were detected. The detection of oxidised Au species was neither expected nor observed, since the etching solution is very dilute and any oxidised Au ions will rapidly dissolve into the solution and be moved away from the X-ray spot by the flow. During the first ~260 minutes there is a gradual linear decrease in the Au 4f signal with time, which is attributable to the accumulation of carbon species on the BLG surface, due to the relatively high base pressure. A sharper decrease is then observed over ~25 minutes until the signal is below the limit of detection for XPS. These changes are shown more clearly in Figure 1D where the Au 4f peak area is plotted for the final 50 minutes of the experiment. Since the XPS probing depth (5λ, for ~99.3% of the signal) for Au is ~8.5 nm at this kinetic energy (λ ~1.7 nm for 1403 eV electrons),<sup>[13–15]</sup> no change in the Au signal is expected until the last ~8.5 nm of Au is reached. Considering this takes ~25 minutes to fully etch, this would suggest a rate of ~0.35 nm/min, assuming uniform etching across the Au surface, and thus 100 nm should take ~285 minutes in good agreement with the total time taken for complete etching following the introduction of the Au etchant.

Figure 1E and F compare the I 3d and O 1s regions respectively before and after the Au film was etched. Note that the cell is filled with water before etching, whereas after etching the Au etching solution continued to flow during XPS characterisation with the chamber pressure remaining at 3×10<sup>-7</sup> mbar. In Figure 1E, prior to etching no iodine signal is detected, whereas after Au etching a clear iodine signal emerges as a result of the etching solution beneath the BLG. The I 3d signal shows

features of multiple chemical species, most likely as a result of simultaneous detection of I<sup>-</sup> and I<sub>3</sub><sup>-</sup> ions from the KI/I<sub>2</sub> solution, as well as contributions from species that have precipitated at graphene defects where water may rapidly evaporate into the vacuum chamber.<sup>[53–57]</sup> We note that ex situ measurements confirm that all of these species can be effectively removed with thorough rinsing in water (see Figure 3C). In Figure 1F both spectra contain a significant contribution at ~530.9 eV associated with contamination on the BLG surface such as hydroxide or oxidised carbon species. The O 1s signal after Au etching shows a high binding energy shoulder around ~533 eV which is tentatively assigned to the liquid-phase water in the cell. Since the binding energy of water is 538.1 eV relative to the vacuum level,<sup>[58]</sup> whereas the binding energies herein are referenced to the Fermi level of graphene, this implies a work function of the Au-SLG window of ~5 eV. This is comparable to the work function estimated from our previous studies of gas-phase species behind Au-SLG windows.<sup>[34]</sup> To gain further confidence that this shoulder is from water and not a result of differential charging, the ratio of O/Si, O/N, and Si/N before and after etching was calculated (see SI for details of calculations). The Si/N ratio increased by 1.3%, while the O/Si ratio increased by 8.2% and the O/N ratio by 7.8%; therefore, this confirms a notable increase in the relative O 1s signal which can be attributed to water now being detectable behind the BLG.

Overall, Figure 1 shows the successful measurement of a BLG-encapsulated flowing liquid in a conventional lab-based XPS system, demonstrating that this approach can be readily extended for use in the many existing systems installed worldwide. Signals from both solute and solvent were recorded through the BLG window whilst the pressure of the vacuum chamber remained at ~3×10<sup>-7</sup> mbar. Given the higher base pressure than typical XPS operating pressures (~10<sup>-9</sup> mbar), some build-up of carbon contamination was observed over the relatively long measurement period.

Figure 2 outlines the method to manufacture the Au (100 nm)/BLG window used above. SLG-coated Cu foil was purchased from PI-KEM (Graphenea), Figure 2(i), and 100 nm of Au was thermally evaporated onto one side to protect the SLG from contamination and provide support during the transfer process. Thermal evaporation was chosen because the energy of the impinging Au atoms is low enough that they do not damage SLG.<sup>[61]</sup> The backside of the Cu was cleaned with an O<sub>2</sub> plasma to ensure there was no residual SLG. Following this a PDMS frame was applied to the Au atop the SLG/Cu.<sup>[50,62,63]</sup> The frame had a hole (~Ø3 mm) punched out that was larger than the window of the SiN<sub>x</sub> membrane (Figure 2(ii)). The PDMS frame was added to minimise wrinkling and ensure the Au/SLG remained taut whilst floating on solutions. The Cu foil was then etched by floating the PDMS/Au/SLG/Cu on a 0.1 M Na<sub>2</sub>S<sub>2</sub>O<sub>8</sub> solution and left for ~3 hours to remove all of the Cu (Figure 2(iii)).<sup>[34,64]</sup> To remove any contamination the PDMS/Au/SLG was transferred to a water bath using a clean piece of SiO<sub>2</sub>(300 nm)/Si wafer where the water bath was refreshed at least three times (Figure 2(iv)). For SLG window manufacture the PDMS/Au/SLG was scooped out of the water using a perforated SiN<sub>x</sub> membrane (ensuring the hole in the PDMS was



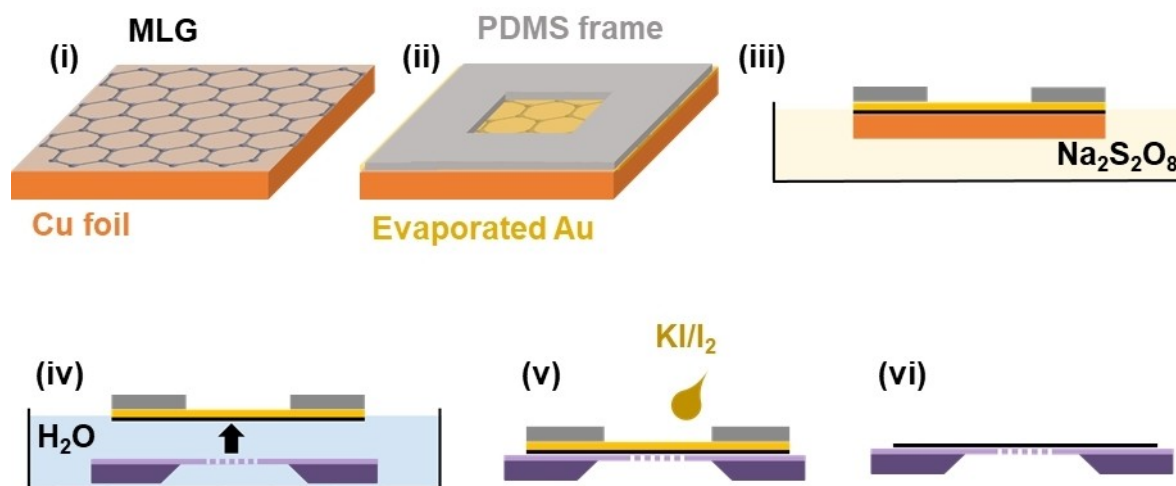


**Figure 2.** Diagram outlining the key steps in transferring (i) SLG from Cu to (vi) a perforated SiN<sub>x</sub> membrane. (ii) Initially 100 nm Au is evaporated onto SLG followed by applying a PDMS frame. (iii) The Cu is then etched in Na<sub>2</sub>S<sub>2</sub>O<sub>8</sub>. (iv) To clean the SLG it is washed in a water bath after etching Cu. PDMS/Au/SLG is scooped out using a SiN<sub>x</sub> membrane and is heated at 40 °C (30 minutes) then 140 °C (30 minutes). (v) The Au can then be removed by etching with KI/I<sub>2</sub> solution. Leaving SLG suspended over the holes in the SiN<sub>x</sub> membrane (vi). If a SLG/Cu piece is used to scoop out the PDMS/Au/SLG at step (iv), and then steps (iii)–(vi) are performed, a BLG window can instead be produced.

aligned with the perforated region) and heated gently at 40 °C for 30 minutes. This dried the surface and removed any residual water trapped between the SLG and SiN<sub>x</sub> which would escape through the edges and help to flatten the PDMS/Au/SLG. Prior to heating, a gentle stream of Ar gas was applied to the surface to help remove large droplets of water. The membrane was then heated at 140 °C to adhere the Au/SLG to the surface to go from step (iv) to (v) in Figure 2. For BLG, once the PDMS/Au/SLG was rinsed with water (Figure 2(iv)) another SLG/Cu piece (with one side cleaned with an O<sub>2</sub> plasma) was used to scoop out the PDMS/Au/SLG instead of a SiN<sub>x</sub> membrane and this was annealed at 40 °C, then 140 °C. The transfer process was then continued by etching the Cu once more (from Figure 2(iii)) and proceeding in the same way as for SLG. Finally, the Au etching solution can be used to remove the Au film if required (Figure 2(v)) followed by rinsing with water. The final result is a perforated SiN<sub>x</sub> membrane with SLG/BLG suspended over the holes, Figure 2(vi).

To confirm the effectiveness of the Au-supported transfer process over large areas, Raman maps were collected from SLG transferred to SiO<sub>2</sub>(300 nm)/Si as shown in Figure 3A, where no additional PDMS support was used. Raman spectra of graphene typically exhibit three main peaks: D (~1350 cm<sup>-1</sup>), G (~1600 cm<sup>-1</sup>), and 2D (~2700 cm<sup>-1</sup>), see Figure S2 for an example Raman spectrum,<sup>[65–68]</sup> and reference<sup>[68]</sup> for more details on the origin of these peaks. High-quality SLG shows a 2D peak fitted by a single Lorentzian function with a FWHM ( $\Gamma_{2D}$ ) of 28–30 cm<sup>-1</sup> and a  $I_{2D}/I_G$  (where  $I$  is the peak height) ratio of  $\geq 2$ .<sup>[69]</sup> The  $I_D/I_G$  ratio is proportional to the level of defects and should therefore be as low as possible. At wrinkles or areas of multi-layered graphene the values of  $\Gamma_{2D}$  and  $I_{2D}/I_G$  are all expected to increase, where  $I_D/I_G$  can decrease at areas where graphene layers overlap but will increase at defective SLG sites.

Figure 3A(i) plots the variation of  $\Gamma_{2D}$  over ~250×185 μm<sup>2</sup> where  $\Gamma_{2D}$  is consistent with SLG over most of the area with a

mean value of 29.5 cm<sup>-1</sup>.  $I_{2D}/I_G$  is similarly uniform at ~2 for most of the area. However wrinkles and small spots are apparent where  $\Gamma_{2D}$  exceeds 40 cm<sup>-1</sup> and  $I_{2D}/I_G$  increases to above 3, consistent with the effects of strain and turbostratic stacking of the wrinkled graphene. For the majority of the surface  $I_D/I_G \leq 0.05$ , but at the same wrinkles and spots there is an increase of  $I_D/I_G$  to above 0.2. Raman mapping thus confirms that the majority of the surface is defect-free SLG. The wrinkles are likely caused during the transfer process, particularly as the PDMS support was not used for this sample. The spots may relate to local contamination as well as small tears/defects, with the later potentially leading to leaks if used to seal the cell. The BLG transfer approach therefore helps to minimise such leaks, as the likelihood of the tears being spatially aligned is vanishingly small.

The uniformity of SLG transferred to a perforated SiN<sub>x</sub> membrane using a PDMS/Au support was measured using SEM (Figure 3B). Figure 3B(i) shows a region away from the window which is covered in SLG, where the fine thread-like features correspond to wrinkles. Wrinkling cannot be completely avoided, given the Cu foils used as templates for SLG growth are relatively rough compared to the SiN<sub>x</sub> membrane. The dark spots are from additional graphene layers which may include residual graphene from the backside of the Cu which was not fully removed by the O<sub>2</sub> plasma cleaning. Figure 3B(ii) shows that the extent of wrinkling is sufficiently low to not significantly impact the coverage of perforations in the SiN<sub>x</sub> membrane. A few holes which are not covered by SLG appear darker and are indicated by the dashed red circles, whilst the black oval indicates some holes that have BLG coverage (as shown by lower contrast with the SiN<sub>x</sub> support). Using the image in Figure 3B(ii) the approximate coverage of SLG over the holes is >98% and the reliability of producing this coverage was ~95% (sample size of >50 membranes). Comparing Figure 3A and 3B, we note that using the PDMS frame led

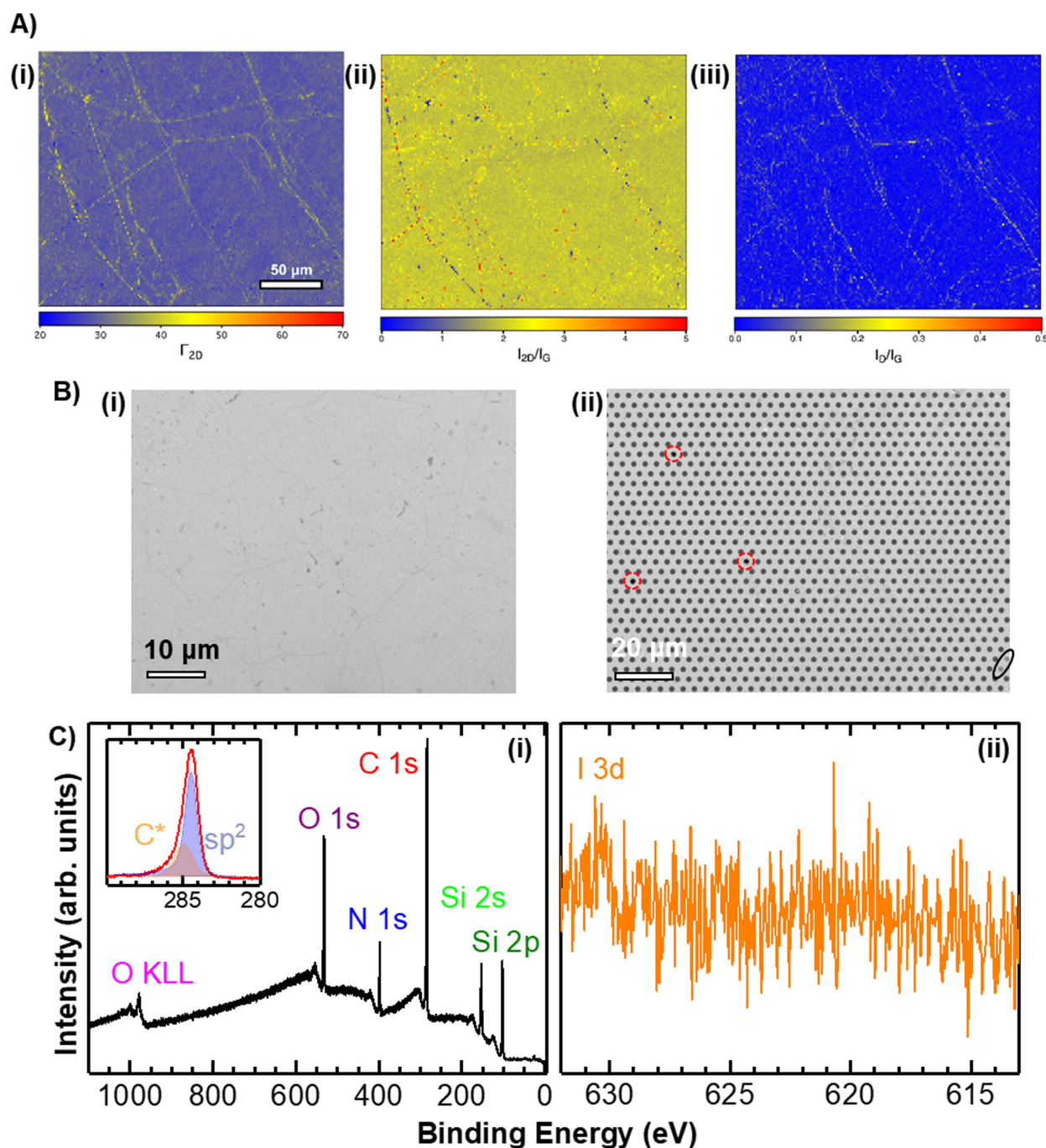


**Figure 3.** (A) Raman maps of SLG transferred to SiO<sub>2</sub>(300 nm)/Si using a Au support layer (without PDMS frame), (i) FWHM ( $\Gamma_{2D}$ ) of the 2D peak, (ii)  $I_D/I_G$ , (iii)  $I_{2D}/I_G$ . (B) SEM collected at 2 keV electron beam energy of SLG transferred to a perforated Si<sub>N</sub>x membrane using a PDMS/Au support, (i) area away from the window, (ii) area of the window showing very few uncovered holes (> 98% coverage). (C) XPS spectra of SLG on the perforated Si<sub>N</sub>x window after PDMS/Au support transfer, (i) survey spectrum showing no additional peaks from contamination, the inset shows the C 1s region, (ii) I 3d region showing no iodine contamination from the Au etching solution.

to a visibly lower extent of wrinkling (particularly those on a large scale), thus demonstrating the improvement the PDMS frame makes to the transfer process. It was important to leave an area without support from the PDMS, as when the PDMS is removed it often removes the Au/graphene beneath it.

Figure 3C(i) shows an XPS survey spectrum of the same sample imaged in SEM (Figure 3B) to determine the extent of contamination from the transfer process. This was collected

from the SLG window of the perforated Si<sub>N</sub>x membrane (using an Al K $\alpha$  X-ray source, 1486.7 eV) with the sp<sup>2</sup> carbon peak set to 284.4 eV for energy calibration. The O KLL Auger features seen at ~979 eV (~507 eV kinetic energy) and O 1s core level at 532.5 eV are consistent with the presence of hydroxide and oxidised carbon species associated with exposure to atmosphere and the aqueous solutions used for transfer (see Figure S3 in the SI). The core level peaks of N 1s at ~398 eV, Si 2s

at ~153 eV, and Si 2p at ~102 eV are attributable to the SiN<sub>x</sub> from the membrane. A strong C 1s core level peak is seen at ~284 eV, with the inset in Figure 3C(i) showing a higher resolution scan of this region. This is well-fitted with two components: the sp<sup>2</sup> hybridised peak (~284.4 eV) arises from the SLG, and the C\* peak (~285.0 eV) is attributable to C–H/C–O species associated with adsorbed surface contaminants e.g. (oxygenated) hydrocarbons.<sup>[34,49,70]</sup> O and C contamination is very difficult to fully avoid, especially considering SLG has been exposed to the atmosphere and several solutions during the transfer, but we note the C contamination is low relative to the sp<sup>2</sup> peak associated with SLG. Detailed regions in XPS were also collected to check for other contaminants from the transfer process. Figure 3C(ii) shows the I 3d region, where there is no detectable iodine species after transfer, indicating effective removal by thorough washing. Detailed scans of the other regions (Na 1s, K 2p, and S 2s) also showed no detectable signal in XPS, thus confirming minimal contamination (see Figure S3 in the SI). The Au 4f and Cu 2p regions confirm no metal traces from Cu or Au, therefore showing no residual metal remains.

The characterisation shown in Figure 3 demonstrates that the PDMS/Au-supported transfer technique, outlined in Figure 2, reliably produces high-quality, continuous, and clean

graphene, and is thus well suited to sealing environmental cells for *in situ* and *operando* studies.

To test the performance of these SLG windows for probing solid/gas interfaces, Cu NPs (~10 nm) were deposited onto the window using a magnetron sputtering gas aggregation (MSGGA) nanoparticle deposition system (Nikalyte Ltd.). The gas flow cell design used is described in more detail in reference<sup>[9]</sup>. The inlet and outlet of the cell enable gas flow and switching of gas compositions for *in situ* measurements. The SiN<sub>x</sub> membrane was placed on top of a graphite gasket to seal it to the rest of the cell. Although less leak-tight than Viton O-rings, graphite gaskets allow for higher temperature heating, although this capability was not exploited herein. Measurements were performed using a NAP-XPS system at Diamond Light Source (B07-C), meaning some gas leakage through the graphite gasket was manageable.<sup>[71]</sup>

Figure 4A shows (i) Cu L<sub>3</sub>-edge NEXAFS spectra acquired in total electron yield (TEY) mode, and corresponding (ii) C 1s and (iii) O 1s XP spectra. All XP spectra in Figure 4A have been normalised to the peak maximum in the relevant region and the Cu L<sub>3</sub>-edge has been normalised to the post-edge. The Cu L<sub>3</sub>-edge spectra have been energy calibrated to align the main peak measured in Ar to 933.7 eV,<sup>[72]</sup> and the C 1s and O 1s spectra were energy calibrated such that the SLG feature in the

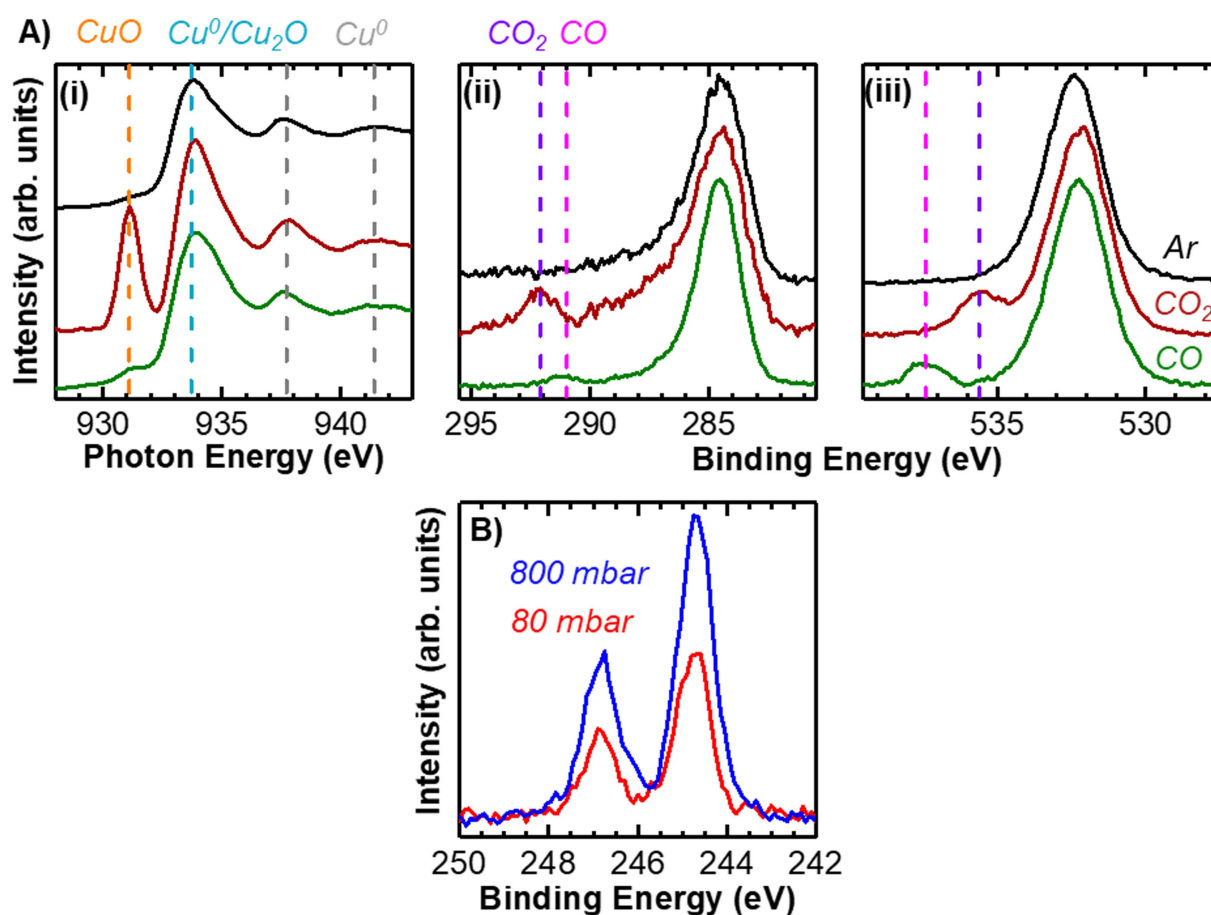


**Figure 4.** NEXAFS/XP spectra collected from Cu NPs (~10 nm) on SLG with gas enclosed within the environmental cell. (A) (i) Cu L<sub>3</sub>-edge, (ii) C 1s, and (iii) O 1s spectra from Cu NPs (~10 nm) exposed to Ar (black), CO<sub>2</sub> (red), and CO (green) at 50 mbar and room temperature. (B) Ar 2p of Ar gas flowed to obtain a pressure of 80 mbar (red) and 800 mbar (blue).



C 1s region is at 284.4 eV. XP spectra were collected at a photon energy of 1700 eV. The Cu  $2p_{3/2}$  region was also measured (Figure S4 in the SI), however the signal was weak and the Cu LMM Auger signal could not be adequately detected. This is attributable to low loadings of Cu NPs used in this study. Cu  $L_{3-}$  edge NEXAFS spectroscopy in TEY mode has higher sensitivity and hence was used to determine oxidation state changes in Cu. Gases were flowed to obtain a pressure of 50 mbar in the cell and dosed in the following order at room temperature: Ar,  $CO_2$ , CO. Initially, under an Ar atmosphere the Cu  $L_{3-}$  edge (Figure 4A(i)) has an edge at 933.7 eV and additional features at 938.0 and 941.8 eV. The peak at 933.7 eV is observed for both  $Cu^0$  and  $Cu^+$  since they have fully occupied 3d orbitals so the excited transition is from the 2p to the 4s orbital.<sup>[73]</sup>  $Cu^0$  and  $Cu^+$  in  $Cu_2O$  can be distinguished by the prominent features seen at 937.7 and 941.4 eV for  $Cu^0$ , and the more step-like absorption edge for  $Cu^0$  compared to the peak-like edge for  $Cu_2O$ .<sup>[74]</sup> Initially under Ar, the Cu  $L_{3-}$  edge indicates the Cu NPs contain a mix of  $Cu_2O$  and  $Cu^0$ . The Cu NPs were exposed to air prior to the experiment leading to oxidation, though as we have previously shown, X-ray beam exposure in a reducing atmosphere can lead to Cu reduction, accounting for the lack of CuO seen under Ar.<sup>[34]</sup> Under Ar gas flow, both the C 1s and O 1s regions (Figure 4A(ii) and (iii)) show broad peaks at ~284.5 eV and ~532.2 eV respectively which are primarily attributable to the SLG and surface contamination on the SLG and  $SiN_x$ .

Upon switching from Ar to  $CO_2$ , the Cu  $L_{3-}$  edge shows a new peak at 931.1 eV indicating CuO formation.  $Cu^{2+}$  has a 3d<sup>9</sup> electron configuration therefore the available transition to the 3d orbital shifts the absorption peak away from  $Cu^0$  and  $Cu^+$ .<sup>[73,75,76]</sup> The higher photon energy features from  $Cu^0$  remain, but the edge at 933.7 eV has become more peak-like in shape suggesting more  $Cu_2O$  formation. This is consistent with the  $CO_2$  oxidising the accessible outside layer of the Cu NPs to CuO with accompanying  $Cu_2O$  formation.<sup>[77,78]</sup> Some  $Cu^0$  is detected from the centre of the Cu NPs which is not exposed to  $CO_2$ , hence explaining the mixture of Cu,  $Cu_2O$ , and CuO seen under 50 mbar of  $CO_2$ . A new peak also appears in the C 1s (292.1 eV) and O 1s (535.6 eV) which can be assigned to the gas-phase  $CO_2$  species.<sup>[9]</sup>

Changing the gas composition to pure CO largely removes the CuO feature from the Cu  $L_{3-}$  edge and causes the edge at 933.7 eV to become more step-like; the Cu oxidation state appears similar in Ar and CO at 50 mbar. CO is highly reducing so will result in mainly  $Cu^0$  on the surface of Cu NPs. The gas-phase peaks in C 1s and O 1s now appear at 291.0 eV and 537.4 eV respectively which correspond to the gas phase peaks for CO which are shifted compared to  $CO_2$ .<sup>[9]</sup>

These measurements highlight a key-benefit of XPS for these systems, where the gas-phase and surface C and O species are well separated from each other, which is not the case in NEXAFS, where it can be challenging to extract information on surface species in high pressure gas environments. Critical to the detection of these species in the C 1s and O 1s regions herein is the use of SLG/BLG windows which are transparent to the low kinetic energy photoelectrons produced

by soft X-ray excitation. The photoionization cross-section of these elements is typically too low at higher photon energies to be reliably detected over a suitably short timescale with hard XPS approaches.<sup>[79]</sup> However, we note that the C and O 1s signals of surface species on the NPs can potentially be obscured by peaks related to graphene and adsorbed contamination.

Careful inspection of the O 1s spectrum indicates slight energy shifts in the main broad peak on changing between the different gases. We note that the features of Cu oxide overlap with the broad peak in the O 1s, as such, oxidation/reduction could contribute to these shifts.<sup>[80–82]</sup> Furthermore, the C 1s binding energy of SLG, which is used here for energy calibration, can vary due to charge transfer doping by the Cu nanoparticles depending on their chemical state, and can thus shift the apparent position of the O 1s peaks.<sup>[34]</sup> We also note that significant proportions of the C and O signals likely arise from contamination on the vacuum side of the window ( $SiN_x$ ); and thus these shifts may instead reflect small changes in charge-dissipation of species on the insulating  $SiN_x$ .

To test the pressure capabilities of the suspended SLG the gas composition was switched back to Ar and the pressure gradually increased. Figure 4B shows the Ar  $2p$  peaks at 80 mbar and 800 mbar, without additional normalisation and with the energy calibrated by setting the gas-phase peak for Ar  $2p_{3/2}$  to 244.7 eV.<sup>[83]</sup> The intensity of the Ar  $2p$  peak at 800 mbar is nearly double that when the pressure is 80 mbar, indicating a greater number of Ar atoms near the graphene window, thus confirming the greater pressure present in the cell. The pressure in the cell was increased to 1 bar with the vacuum chamber pressure remaining at  $\sim 5 \times 10^{-2}$  mbar, whereas under 50 mbar in the cell the pressure of the vacuum chamber was  $\sim 1 \times 10^{-2}$  mbar. The pressure and signal increase are not directly proportional as a larger pressure in the cell will increase the scattering of photoelectrons. To perform conventional lab-based XPS gas-phase measurements, leakage through the graphite gasket could be reduced by using Viton O-rings (if high-temperature heating isn't required) or another sealing method. Leakage across the window could also be reduced by using BLG rather than SLG.

The success of BLG in sealing an aqueous solution in a conventional lab-based XPS system and SLG in sealing a gas within a NAP-XPS system show the potential of the PDMS/Au-supported transfer process for producing continuous, clean graphene windows in a reliable manner, which has been an outstanding challenge in the application of graphene-sealed environmental reaction cells.<sup>[84]</sup> A possible future application of this is sealing an environmental cell for *in situ* measurements with a high-pressure gas environment even in conventional lab-based XPS systems: using a Au/BLG window, the approach shown in Figure 1 can be used to align the active area, etch the Au, and then the solution can be replaced with gas flow (after cleaning of the BLG with water).



## Conclusions

A PDMS/Au-supported transfer process is demonstrated to reliably produce continuous, high-quality and contamination-free suspended SLG/BLG windows over perforated SiN<sub>x</sub> membranes. These windows were used to perform *in situ* measurements of Au etching using an aqueous solution where an etching rate of ~0.35 nm/min was determined and a signal from the solid/liquid interface was measured in a conventional lab-based XPS system. The PDMS/Au-supported transfer method was shown to successfully seal a reaction cell filled with high-pressure (~1 bar) gas for measurement in a NAP-XPS system. There appears no fundamental barrier to reaching pressures well above 1 bar (particularly with a BLG window) in a NAP system, or reaching pressures of 1 bar in conventional lab-based systems if suitable adjustments are made to how the reaction cell is sealed. This would help significantly widen access to *in situ* and *operando* XPS measurements of catalytic reactions under increasingly realistic conditions.

## Supporting Information

The Supporting Information contains: a detailed experimental section, calculation of atomic ratios for liquid XPS experiments, an example Raman spectrum of SLG, additional XPS regions from the transfer of SLG, Cu 2p<sub>3/2</sub> regions from XPS of Cu NPs at 50 mbar, and O 1s, C 1s, and Ar 2p regions from Figure 4 without a Shirley background subtraction applied.

## Acknowledgements

The authors acknowledge funding from the European Research Council (ERC) under the European Union's Horizon 2020 research and innovation programme (EXISTAR, grant agreement No. 950598) and the Engineering and Physical Science Research Council (EPSRC) through grants EP/T001038/1, and EP/R010145/1 (Henry Royce Institute). R.S.W. acknowledges a CAMS-UK Fellowship through the Analytical Chemistry Trust Fund and a UKRI Future Leaders Fellowship (MR/V024558/1). E.S.J. acknowledges a Clarendon Scholarship and a Trinity College Scholarship. We thank Diamond Light Source for beamtime on beamline B07-C under proposal SI30358. The UK Catalysis Hub is thanked for resources and support provided via our membership of the UK Catalysis Hub Consortium funded by EPSRC grant: EP/R026815/1. X-ray photoelectron (XPS) data was acquired at the EPSRC National Facility for XPS ("HarwellXPS", EP/Y023587/1, EP/Y023609/1, EP/Y023536/1, EP/Y023552/1 and EP/Y023544/1), operated by Cardiff University and UCL, under Contract No. PR16195.

## Conflict of Interests

The authors declare no conflict of interest.

## Data Availability Statement

The data that support the findings of this study are available from the corresponding author upon reasonable request.

**Keywords:** Graphene · X-ray Photoelectron Spectroscopy · *In situ* · Transfer · Ambient Pressure

- [1] Y. Li and Z. Wu, *Catal. Today* **2023**, 420, 114029.
- [2] D. Liu, Z. Shadike, R. Lin, K. Qian, H. Li, K. Li, S. Wang, Q. Yu, M. Liu, S. Ganapathy, X. Qin, Q. H. Yang, M. Wagemaker, F. Kang, X. Q. Yang, B. Li, *Adv. Mater.* **2019**, 31, 1806620.
- [3] J. Maibach, J. Rizell, A. Matic, N. Mozhzhukhina, *ACS Materials Lett.* **2023**, 5, 2431–2444.
- [4] J. Schnadt, J. Knudsen, N. Johansson, *J. Phys. Condens. Matter* **2020**, 32, 413003.
- [5] C. H. Wu, R. S. Weatherup, M. B. Salmeron, *Phys. Chem. Chem. Phys.* **2015**, 17, 30229–30239.
- [6] A. Kolmakov, L. Gregoratti, M. Kiskinova, S. Günther, *Top. Catal.* **2016**, 59, 448–468.
- [7] Y. Han, H. Zhang, Y. Yu, Z. Liu, *ACS Catal.* **2021**, 11, 1464–1484.
- [8] A. Beck, M. Zabilskiy, M. A. Newton, O. Safonova, M. G. Willinger, J. A. van Bokhoven, *Nat. Catal.* **2021**, 4, 488–497.
- [9] J. E. N. Swallow, E. S. Jones, A. R. Head, J. S. Gibson, R. Ben David, M. W. Fraser, M. A. van Spronsen, S. Xu, G. Held, B. Eren, R. S. Weatherup, *J. Am. Chem. Soc.* **2023**, 145, 6730–6740.
- [10] B. Eren, C. G. Sole, J. S. Lacasa, D. Grinter, F. Venturini, G. Held, C. S. Esconjauregui, R. S. Weatherup, *Phys. Chem. Chem. Phys.* **2020**, 22, 18806–18814.
- [11] P. Jiang, J. L. Chen, F. Borondics, P. A. Glans, M. W. West, C. L. Chang, M. Salmeron, J. Guo, *Electrochem. Commun.* **2010**, 12, 820–822.
- [12] F. A. Stevie, C. L. Donley, *J. Vac. Sci. Technol. A: Vacuum, Surfaces, Films* **2020**, 38, 063204.
- [13] S. Tanuma, C. J. Powell, D. R. Penn, *Surf. Interface Anal.* **2011**, 43, 689–713.
- [14] S. Tanuma, C. J. Powell, D. R. Penn, *Surf. Interface Anal.* **1993**, 21, 165–176.
- [15] M. P. Seah, W. A. Dench, *Surf. Interface Anal.* **1979**, 1, 2–11.
- [16] E. S. Jones, J. E. N. Swallow, R. S. Weatherup, *ACS Symp. Ser.* **2021**, 1396, 175–218.
- [17] H. Siegbahn, K. Siegbahn, *J. Electron Spectrosc. Relat. Phenom.* **1973**, 2, 319–325.
- [18] K. Siegbahn, C. Nordling, G. Johansson, J. Hedman, P. F. Hedén, K. Hamrin, U. Gelius, T. Bergmark, L. O. Werme, R. Manne, Y. Baer, *ESCA applied to free molecules*, North-Holland Publishing Company, Amsterdam-London, **1969**.
- [19] J. J. Pireaux, S. Svensson, E. Basilier, P. Å. Malmqvist, U. Gelius, R. Caudano, K. Siegbahn, *Phys. Rev. A* **1976**, 14, 2133–2146.
- [20] D. F. Ogletree, H. Bluhm, G. Lebedev, C. S. Fadley, Z. Hussain, M. Salmeron, *Rev. Sci. Instrum.* **2002**, 73, 3872.
- [21] S. Axnanda, E. J. Crumlin, B. Mao, S. Rani, R. Chang, P. G. Karlsson, M. O. M. Edwards, M. Lundqvist, R. Moberg, P. Ross, Z. Hussain, Z. Liu, *Sci. Rep.* **2015**, 5, 9788.
- [22] T. Masuda, H. Yoshikawa, H. Noguchi, T. Kawasaki, M. Kobata, K. Kobayashi, K. Uosaki, *Appl. Phys. Lett.* **2013**, 103, 111605.
- [23] C. Schlueter, A. Gloskovskii, K. Ederer, I. Schostak, S. Piec, I. Sarkar, Y. Matveyev, P. Lömker, M. Sing, R. Claessen, C. Wiemann, C. M. Schneider, K. Medjanik, G. Schönhense, P. Amann, A. Nilsson, W. Drube, *AIP Conf. Proc.* **2019**, 2054, 040010.
- [24] J. J. Yeh, I. Lindau, *At. Data Nucl. Data Tables* **1985**, 32, 1–155.
- [25] J. J. Velasco-Velez, L. J. Falling, D. Bernsmeier, M. J. Sear, P. C. J. Clark, T. S. Chan, E. Stotz, M. Hävecker, R. Kraehnert, A. Knop-Gericke, C. H. Chuang, D. E. Starr, M. Favaro, R. V. Mom, *J. Phys. D* **2021**, 54, 124003.
- [26] S. K. Beaumont, *Phys. Chem. Chem. Phys.* **2020**, 22, 18747–18756.
- [27] S. Khatun, S. R. Cohen, S. S. Peled, I. Rosenhek-Goldian, R. S. Weatherup, B. Eren, *Adv. Mater. Interfaces* **2021**, 8, 2100662.
- [28] S. Khatun, M. A. Andrés, S. R. Cohen, I. Kaplan-Ashiri, O. Brontvein, I. Rosenhek-Goldian, R. S. Weatherup, B. Eren, *Electrochim. Acta* **2022**, 431, 141145.
- [29] R. Endo, D. Watanabe, M. Shimomura, T. Masuda, *Appl. Phys. Lett.* **2019**, 114, 173702.

- [30] A. Kolmakov, D. A. Dikin, L. J. Cote, J. Huang, M. K. Abyaneh, M. Amati, L. Gregoratti, S. Günther, M. Kiskinova, *Nat. Nanotechnol.* **2011**, *6*, 651–657.
- [31] S. Nemšák, E. Strelcov, T. Duchoň, H. Guo, J. Hackl, A. Yulaev, I. Vlassiouk, D. N. Mueller, C. M. Schneider, A. Kolmakov, *J. Am. Chem. Soc.* **2017**, *139*, 18138–18141.
- [32] H. Guo, E. Strelcov, A. Yulaev, J. Wang, N. Appathurai, S. Urquhart, J. Vinson, S. Sahu, M. Zvolak, A. Kolmakov, *Nano Lett.* **2017**, *17*, 1034–1041.
- [33] J. J. Velasco-Velez, V. Pfeifer, M. Hävecker, R. S. Weatherup, R. Arrigo, C. H. Chuang, E. Stotz, G. Weinberg, M. Salmeron, R. Schlögl, A. Knop-Gericke, *Angew. Chem. Int. Ed.* **2015**, *54*, 14554–14558.
- [34] R. S. Weatherup, B. Eren, Y. Hao, H. Bluhm, M. B. Salmeron, *J. Phys. Chem. Lett.* **2016**, *7*, 1622–1627.
- [35] J. J. Velasco-Vélez, V. Pfeifer, M. Hävecker, R. Wang, A. Centeno, A. Zurutuza, G. Algara-Siller, E. Stotz, K. Skorupska, D. Teschner, P. Kube, P. Braeuninger-Weimer, S. Hofmann, R. Schlögl, A. Knop-Gericke, *Rev. Sci. Instrum.* **2016**, *87*, 053121.
- [36] J. Kraus, R. Reichelt, S. Günther, L. Gregoratti, M. Amati, M. Kiskinova, A. Yulaev, I. Vlassiouk, A. Kolmakov, *Nanoscale* **2014**, *6*, 14394–14403.
- [37] A. Yulaev, H. Guo, E. Strelcov, L. Chen, I. Vlassiouk, A. Kolmakov, *ACS Appl. Mater. Interfaces* **2017**, *9*, 26492–26502.
- [38] E. Tsunemi, Y. Watanabe, H. Oji, Y. T. Cui, J. Y. Son, A. Nakajima, *J. Appl. Phys.* **2015**, *117*, 234902.
- [39] T. Masuda, *Top. Catal.* **2018**, *61*, 2103–2113.
- [40] J. S. Bunch, S. S. Verbridge, J. S. Alden, A. M. Van Der Zande, J. M. Parpia, H. G. Craighead, P. L. McEuen, *Nano Lett.* **2008**, *8*, 2458–2462.
- [41] R. S. Weatherup, *Top. Catal.* **2018**, *61*, 2085–2102.
- [42] P. Leidinger, J. Kraus, T. Kratky, P. Zeller, T. O. Menteş, F. Genuzio, A. Locatelli, S. Günther, *J. Phys. D* **2021**, *54*, 234001.
- [43] S. Xu, L. Zhang, B. Wang, R. S. Ruoff, *Cell Reports Phys. Sci.* **2021**, *2*, 100372.
- [44] X. Zhang, J. Lai, T. Gray, *Oxford Open Mater. Sci.* **2023**, *3*, 1–14.
- [45] L. P. Ma, W. Ren, H. M. Cheng, *Small Methods* **2019**, *3*, 1900049.
- [46] M. Chen, R. C. Haddon, R. Yan, E. Bekyarova, *Mater. Horiz.* **2017**, *4*, 1054–1063.
- [47] M. Kratzer, B. C. Bayer, P. R. Kidambi, A. Matković, R. Gajić, A. Cabrero-Vilatela, R. S. Weatherup, S. Hofmann, C. Teichert, *Appl. Phys. Lett.* **2015**, *106*, 103101.
- [48] A. Yulaev, G. Cheng, A. R. Hight Walker, I. V. Vlassiouk, A. Myers, M. S. Leite, A. Kolmakov, *RSC Adv.* **2016**, *6*, 83954–83962.
- [49] W. H. Lin, T. H. Chen, J. K. Chang, J. I. Taur, Y. Y. Lo, W. L. Lee, C. S. Chang, W. Bin Su, C. I. Wu, *ACS Nano* **2014**, *8*, 1784–1791.
- [50] S. Unarunotai, Y. Murata, C. E. Chialvo, H. S. Kim, S. MacLaren, N. Mason, I. Petrov, J. A. Rogers, *Appl. Phys. Lett.* **2009**, *95*, 202101.
- [51] S. B. Desai, S. R. Madhvapathy, M. Amani, D. Kiriya, M. Hettick, M. Tosun, Y. Zhou, M. Dubey, J. W. Ager, D. Chrzan, A. Javey, *Adv. Mater.* **2016**, *28*, 4053–4058.
- [52] T. A. Green, *Gold Bull.* **2014**, *47*, 205–216.
- [53] P. Ahlberg, M. Hinnemo, M. Song, X. Gao, J. Olsson, S. L. Zhang, Z. B. Zhang, *Appl. Phys. Lett.* **2015**, *107*, 203104.
- [54] W. R. Salaneck, H. R. Thomas, R. W. Bigelow, C. B. Duke, E. W. Plummer, A. J. Heeger, A. G. Macdiarmid, *J. Chem. Phys.* **1980**, *3678*, 3674–3678.
- [55] M. S. Ahsan, V. Kochetov, D. Hein, S. I. Bokarev, I. Wilkinson, *Phys. Chem. Chem. Phys.* **2022**, *24*, 15540–15555.
- [56] D. Zheng, C. N. Young, W. F. Stickle, *Surf. Sci. Spectra* **2023**, *30*, 024026.
- [57] N. Ottosson, M. Faubel, S. E. Bradforth, P. Jungwirth, B. Winter, *J. Electron Spectrosc. Relat. Phenom.* **2010**, *177*, 60–70.
- [58] B. Winter, E. F. Aziz, U. Hergenhausen, M. Faubel, I. V. Hertel, *J. Chem. Phys.* **2007**, *126*, 124504.
- [59] M. A. Brown, B. Winter, M. Faubel, J. C. Hemminger, *J. Am. Chem. Soc.* **2009**, *131*, 8354–8355.
- [60] M. J. Krisch, R. D'Auria, M. A. Brown, D. J. Tobias, J. C. Hemminger, M. Ammann, D. E. Starr, H. Bluhm, *J. Phys. Chem. C* **2007**, *111*, 13497–13509.
- [61] J. S. Gibson, S. Narayanan, J. E. N. Swallow, P. Kumar-Thakur, M. Pasta, T.-L. Lee, R. S. Weatherup, *Faraday Discuss.* **2022**, *236*, 267–287.
- [62] J. Seo, C. Kim, B. S. Ma, T. I. Lee, J. H. Bong, J. G. Oh, B. J. Cho, T. S. Kim, *Adv. Funct. Mater.* **2018**, *28*, 1707102.
- [63] S. Cha, M. Cha, S. Lee, J. H. Kang, C. Kim, *Sci. Rep.* **2015**, *5*, 17877.
- [64] L. Zheng, Y. Chen, N. Li, J. Zhang, N. Liu, J. Liu, W. Dang, B. Deng, Y. Li, X. Gao, C. Tan, Z. Yang, S. Xu, M. Wang, H. Yang, L. Sun, Y. Cui, X. Wei, P. Gao, H.-W. Wang, H. Peng, *Nat. Commun.* **2020**, *11*, 541.
- [65] F. Tuinstra, J. L. Koenig, *J. Chem. Phys.* **1970**, *53*, 1126–1130.
- [66] C. Thomsen, S. Reich, *Phys. Rev. Lett.* **2000**, *85*, 5214–5217.
- [67] J.-B. Wu, M.-L. Lin, X. Cong, H.-N. Liu, P.-H. Tan, *Chem. Soc. Rev.* **2018**, *47*, 1822–1873.
- [68] A. C. Ferrari, D. M. Basko, *Nat. Nanotechnol.* **2013**, *8*, 235–246.
- [69] H. C. Lee, W. W. Liu, S. P. Chai, A. R. Mohamed, A. Aziz, C. S. Khe, N. M. S. Hidayah, U. Hashim, *RSC Adv.* **2017**, *7*, 15644–15693.
- [70] R. S. Weatherup, L. D'Arisei, A. Cabrero-Vilatela, S. Caneva, R. Blume, J. Robertson, R. Schloegl, S. Hofmann, *J. Am. Chem. Soc.* **2015**, *137*, 14358–14366.
- [71] D. C. Grinter, F. Venturini, P. Ferrer, M. A. van Spronsen, R. Arrigo, W. Quevedo Garzon, K. Roy, A. I. Large, S. Kumar, G. Held, *Synchrotron Radiat. News* **2022**, *35*, 39–47.
- [72] P. Jiang, D. Prendergast, F. Borondics, S. Porsgaard, L. Giovanetti, E. Pach, J. Newberg, H. Bluhm, F. Besenbacher, M. Salmeron, *J. Chem. Phys.* **2013**, *138*, 024704.
- [73] P. Thakur, V. Bisogni, J. C. Cezar, N. B. Brookes, G. Ghiringhelli, S. Gautam, K. H. Chae, M. Subramanian, R. Jayavel, K. Asokan, *J. Appl. Phys.* **2010**, *107*, 103915.
- [74] A. Jonas, H. Stiel, L. Glöggler, D. Dahm, K. Dammer, B. Kanngießer, I. Mantouvalou, *Opt. Express* **2019**, *27*, 36524–36537.
- [75] D. D. Sarma, O. Strebel, C. T. Simmons, U. Neukirch, G. Kaindl, R. Hoppe, H. P. Müller, *Phys. Rev. B* **1988**, *37*, 9784–9787.
- [76] P. F. Schofield, C. M. B. Henderson, S. A. T. Redfern, G. van der Laan, *Phys. Chem. Miner.* **1993**, *20*, 375–381.
- [77] R. S. Weatherup, C. H. Wu, C. Escudero, V. Pérez-Dieste, M. B. Salmeron, *J. Phys. Chem. B* **2018**, *122*, 737–744.
- [78] B. Eren, R. S. Weatherup, N. Liakakos, G. A. Somorjai, M. Salmeron, et al., *J. Am. Chem. Soc.* **2016**, *138*, 8207–8211.
- [79] P. Amann, B. Klötzer, D. Degerman, N. Köpfle, T. Götsch, P. Lömker, C. Rameshan, K. Ploner, D. Bikaljevic, H. Wang, M. Soldemo, M. Shipilin, C. M. Goodwin, J. Gladh, J. H. Stenlid, M. Börner, C. Schlueter, A. Nilsson *Science* **2022**, *376*, 603–608.
- [80] M. C. Biesinger, *Surf. Interface Anal.* **2017**, *49*, 1325–1334.
- [81] L. Trotochaud, A. R. Head, S. Pletincx, O. Karsloğlu, Y. Yu, A. Waldner, L. Kyhl, T. Hauffman, H. Terry, B. Eichhorn, H. Bluhm, *J. Phys. Chem. B* **2018**, *122*, 1000–1008.
- [82] B. Eren, C. Heine, H. Bluhm, G. A. Somorjai, M. Salmeron, *J. Am. Chem. Soc.* **2015**, *137*, 11186–11190.
- [83] D. I. Patel, S. Bahr, P. Dietrich, M. Meyer, A. Thißen, M. R. Linford, *Surf. Sci. Spectra* **2019**, *26*, 014024.
- [84] R. Arrigo, D. Aureau, P. Bhatt, M. A. Buckingham, J. J. C. Counter, G. D'Acunto, P. R. Davies, D. A. Evans, W. R. Flavell, J. S. Gibson, S. Guan, G. Held, M. Isaacs, J. M. Kahk, C. F. P. Kastorp, H. Kersell, A. Krizan, A. I. Large, R. Lindsay, J. Lischner, P. Lömker, D. Morgan, S. Nemšák, A. Nilsson, D. Payne, B. P. Reed, O. Renault, G. Rupprechter, A. G. Shard, M. Shoji, M. G. Silly, W. S. J. Skinner, F. Solal, K. A. Stoerzinger, S. Suzer, J. J. Velasco-Vélez, M. Walker, R. S. Weatherup, *Faraday Discuss.* **2022**, *236*, 219–266.

Manuscript received: February 1, 2024

Revised manuscript received: April 14, 2024

Accepted manuscript online: April 21, 2024

Version of record online: June 7, 2024